RSC Advances

PAPER

View Article Online
View Journal | View Issue

Cite this: *RSC Adv.*, 2014, **4**, 32429

A study to initiate development of sustainable Ni/γ-Al_2O_3 catalyst for hydrogen production from steam reforming of biomass-derived glycerol

Gullapelli Sadanandam, Kasala Ramya, Donthamsetti Bhanu Kishore, Valluri Durgakumari,* Machiraju Subrahmanyam and Komandur V. R. Chary

Received 24th February 2014
Accepted 30th June 2014

DOI: 10.1039/c4ra01612b

www.rsc.org/advances

Glycerol steam reforming, which is a potential technology for hydrogen production in fuel-cell applications, is of great interest to researchers in recent years. Using aqueous glycerol, which is a byproduct in biodiesel production, as a direct feed for steam reforming is a promising method to produce hydrogen. Ni (5, 10, 15, 20 and 25 wt%) loaded on commercial γ-Al_2O_3 by the impregnation method is used to study steam reforming of glycerol. The catalyst was characterized by XRD, EDAX, BET surface area, TPR, NH_3-TPD, TEM, CHNS and Raman techniques. The catalysts are evaluated on time streams for the effect of Ni loading, temperature, and glycerol-to-water mole ratio (GWMRs). Under the parameters investigated, 15 wt% Ni/γ-Al_2O_3 was found to be the most promising catalyst in terms of glycerol conversion and hydrogen production with minimum coking. The characterization of the catalysts clearly establishes that interaction of Ni^{2+} with γ-Al_2O_3 support, Ni^{2+} reducibility, particle size, and acidity of the support are seen governing the stable activity of the catalysts. Thus, a structural activity correlation has been established on the Ni/γ-Al_2O_3 catalysts.

1 Introduction

Because of the depletion of global fossil fuel resources, growing environmental impact and energy security concerns, there is a need to find new alternative routes for hydrogen production.[1–7] There is a significant amount of research being pursued towards the development of H_2 production technologies for fuel-cell applications as fuel cells that consume hydrogen are environmentally clean and highly efficient devices for electrical power generation.[8] The full environmental benefit of generating power from hydrogen fuel cells is achieved when hydrogen is produced from renewable sources like solar power and biomass. In this context, the conversion of cheap and available biomass or biomass-derived byproducts for H_2 production is considered to be a promising approach to meet the requirement of H_2 and realize sustainable development. To date, glycerol has been considered as an alternative fuel for hydrogen production because it is a byproduct of biodiesel production, which uses vegetable oils or fats as feedstock. Hence, in this context, hydrogen production from steam reforming of glycerol appears to be a promising alternative. The reaction that describes the production of hydrogen from glycerol can be expressed as follows:

$$C_3H_8O_3 + 3H_2O \rightarrow 3CO_2 + 7H_2 \quad (1)$$

Inorganic and Physical Chemistry Division, Indian Institute of Chemical Technology, Hyderabad-500 607, India. E-mail: durgakumari@iict.res.in; Fax: +91-40-27160921; Tel: +91-40-27193165

The steam reforming of glycerol to produce hydrogen using catalysts has been investigated in the recent decade.[9–17] The steam reforming of glycerol by noble metal catalysts is expensive, and the use of low-cost non-noble catalysts would be advantageous from an economic standpoint. This reaction is very interesting for its operational characteristics and greater efficiency. Noble metal-supported catalysts are more active and less susceptible to carbon deposition than non-noble metals.[11–13] At an industrial scale, the use of Ni-supported catalysts for steam reforming is interesting because this catalyst is inexpensive and more highly available than noble metals. Both development and stability of Ni-supported catalysts are subjects of investigation.[14,15] Ni-based catalysts are used because of their high efficiency for the cleavage of C–C, O–H, and C–H bonds in hydrocarbons. Moreover, they catalyze the water–gas shift reaction to remove adsorbed CO from the surface of the catalysts.[16] Ce, Mg, Zr, and La modifying Ni/Al_2O_3 enhanced the hydrogen selectivity with minimum coking.[18] More recently, the glycerol steam reforming was evaluated on Ni-supported CeO_2, Al_2O_3, and CeO_2-promoted Al_2O_3, and the incorporation of low ceria loadings enhanced catalytic activity, whereas increasing ceria contents reduced the capacity of the catalyst to convert intermediate oxygenated hydrocarbons into hydrogen.[19]

Ni/Al_2O_3 catalysts suffer deactivation during the steam reforming of oxygenated hydrocarbons due to the formation of carbonaceous deposits and the sintering of the metallic phase. Coke formation is usually related to dehydration,

cracking, and polymerization reactions taking place on the acid sites of Al_2O_3,[20] whereas the sintering of the metallic phase can be associated with a transition of Al_2O_3 to the crystalline phase during a reaction.[21] Using supported catalysts of Rh/Al_2O_3 and Ni on Al_2O_3, MgO, and CeO_2, carbonaceous deposits were formed from olefins, which were produced by the glycerol thermal decomposition, and temperatures above 650 °C favoured the generation of encapsulated carbon that decreases catalyst stability.[22] Using Ni/α-Al_2O_3 and Ni/α-Al_2O_3 modified with ZrO_2 and CeO_2, Ni/α-Al_2O_3-modified CeO_2 catalysts displayed great stability, and its basic characteristic inhibits the reactions that form carbonaceous deposits deactivating the catalyst.[23] On Ni-loaded Al_2O_3, ZrO_2, and CeO_2 catalysts, which are used in glycerol for reforming the stable activity and maximum H_2 selectivity, are observed on Al_2O_3, but the coke formation rate is more on Al_2O_3.[24] The effect of Ni precursors on Al_2O_3 catalysts used in the glycerol reforming reaction was studied, and it was inferred that high Ni dispersion and small Ni particle size promoted catalyst activity.[25]

Previous thermodynamic studies of glycerol-steam systems indicate complete glycerol conversion with a high attainment of H_2 yield.[26–30] These studies also suggest that carbon formation is inhibited at high reaction temperatures (>900 K), low pressure and high steam-to-glycerol ratio (STGR, 12 : 1). Adhikari *et al.* considered the thermodynamic equilibrium analysis for glycerol-steam reforming varying parameters, namely, pressure of 1–5 atm, temperatures at 600–1000 K, and STGR of 1 : 1–9 : 1.[29] The best conditions for producing hydrogen are temperatures higher than 900 K, atmospheric pressure, and a glycerol-to-water mole ratio of 1 : 9 as CH_4 production is minimized and carbon formation is thermodynamically inhibited under these conditions.

In our previous work, we have reported the effect of catalyst size in glycerol steam reforming for H_2 production over Ni/SiO_2, where 2 × 2 and 2 × 4 mm catalysts promote coke formation at high temperatures (600 °C). The higher size of 3 × 5 mm improves the catalytic performance and minimizes coke formation.[31] The present investigation is a part of the ongoing activity on catalyst development for hydrogen production from biomass-derived glycerol for 2–3 kW PEMFC system to meet the immediate requirement of alternate clean energy-based back-up power supply for telecom towers, which were sponsored by the Ministry of New & Renewable Energy (MNRE), Government of India. There is no commercial catalyst available for glycerol reforming, and IICT has initiated catalyst development based on the previous experience from the development of methanol reforming.[32] Ni/γ-Al_2O_3 is a fundamentally well-established system as a catalyst for methane reforming, and glycerol reforming is altogether a new activity with more number of carbon atoms and high coking rate. The present investigation details the preparation, characterization and time on stream activity of Ni/γ-Al_2O_3 catalysts. Moreover, an understanding of the stable and sustainable activity of these catalysts is discussed in terms of acidity, reducibility, Ni crystallite size and coking rate.

2 Materials and methods

2.1 Chemicals

γ-Al_2O_3 extrudated (Engelhard corporation, AL-3996) with a surface area of 192 $m^2\ g^{-1}$, $Ni(NO_3)_2 \cdot 6H_2O$ (Sigma-Aldrich), and glycerol (Qualigens Fine Chemicals Pvt. Ltd. (India)) were used.

2.2 Catalyst preparation

Nickel (5, 10, 15, 20 and 25 wt%) was loaded on γ-Al_2O_3 (4 × 6 mm) by an impregnation method, which is generally used on preformed supports for high dispersion and controlled size of active sites. The method involved addition of γ-Al_2O_3 to a known amount of $Ni(NO_3)_2 \cdot 6H_2O$ dissolved in distilled water. Excess water was evaporated to dryness with constant stirring and slow heating. The dried sample was calcined at 500 °C/5 h in air. The catalysts with 0, 5, 10, 15, 20 and 25 (wt%) of nickel-loaded γ-Al_2O_3 were labelled as A, 5NA, 10NA, 15NA, 20NA and 25NA. The Ni-loaded γ-Al_2O_3 catalysts were used in glycerol steam reforming at glycerol-to-water mole ratio (GWMRs) of 1 : 9 and 650 °C, and the used catalysts were labelled as 5NA-1-9, 10NA-1-9, 15NA-1-9, 20NA-1-9 and 25NA-1-9. A nickel-loaded γ-Al_2O_3 catalyst (15 wt%) was used in glycerol steam reforming at different temperatures (500, 550, 600 and 650 °C using glycerol-to-water mole ratio of 1 : 9) and different GWMRs (1 : 3, 1 : 6 and 1 : 9 at 650 °C) and were labelled as 15NA-500, 15NA-550, 15NA-600, 15NA-650, 15NA-1-3, 15NA-1-6 and 15NA-1-9, respectively.

2.3 Catalyst characterization

The X-ray diffraction (XRD) patterns of the Ni/γ-Al_2O_3 fresh and used catalysts were recorded with Rigaku Miniflex diffractometer with a nickel-filtered Cu Kα radiation (λ = 0.15406 nm) from $2\theta = 5°$–$80°$ with beam voltage and beam currents of 40 kV and 100 mA, respectively. The crystallite sizes of the catalysts were calculated using the Debye-Scherrer equation ($K\lambda/\beta \cos \theta$). Elemental analysis was carried out using Link, ISIS-300, Oxford, energy-dispersive analysis of X-ray spectroscopy (EDAX). The Brunauer–Emmett–Teller (BET) surface areas of fresh and used samples were measured by N_2 adsorption at −196 °C in an Autosorb-I (Quantachrome) instrument. Transmission electron microscopy (TEM) studies were conducted on a TECHNAI 20B2 S-Twin unit operated at 120 kV with a filament current of 28 mA. The carbon contents were estimated using an Elementar vario Microcube (Germany) CHNS analyser and calibrated with sulphanilic acid using samples in duplicate. The sample was dropped into the combustion tube automatically and subjected to combustion temperatures of up to 1200 °C. Complete combustion of all samples was ensured with a special oxygen jet injection of tungsten oxide (catalyst for oxidation). The He carrier gas transfers the combustion gaseous products into the copper tube where nitrogen oxide is reduced to molecular N_2 at 850 °C. The mixture of helium, CO_2, H_2O, and SO_2 are guided to specific adsorption traps and measurements, and nitrogen travels to the TC detector. Confocal micro-Raman spectra were recorded at room temperature in the range of 1000–2000 cm^{-1} using a Horiba Jobin-Yvon Lab Ram HR spectrometer with a

17 mW internal He–Ne (helium–neon) laser source of excitation with a wavelength of 632.8 nm. The catalyst sample in powder form (about 5–10 mg) was usually spread onto a glass slide below the confocal microscope for measurements. Temperature-programmed reduction (TPR) was carried out in a quartz microreactor interfaced to gas chromatography with a thermal conductivity detector (GC with TCD) unit. For the TPR analysis, a catalyst sample of about 50 mg was loaded in an isothermal zone of a quartz reactor (i.d. = 6 mm, length = 30 cm) heated by an electric furnace at a rate of 10 °C min^{-1} to 300 °C in flowing helium gas at a flow rate of 30 ml min^{-1}, which facilitates the desorption of physically adsorbed water. Then, after the sample was cooled to room temperature, helium was switched over to 30 ml min^{-1} reducing gas of 5% H_2 in argon, and the temperature was increased to 1000 °C at a rate of 5 °C min^{-1}. Hydrogen consumption was measured by means of a thermal conductivity detector. The steam formed during the reduction was removed by a molecular sieve trap prior to detection. The acidity of the catalysts was measured by temperature-programmed desorption of ammonia (NH_3-TPD). In a typical experiment, 0.1 g of catalyst was loaded and pretreated in He gas at 300 °C for 2 h. After pretreatment, the temperature was brought to 100 °C, and the adsorption of NH_3 was carried out by passing a mixture of 10% NH_3-balanced He gas over the catalyst for 1 h. The catalyst surface was flushed with He gas at the same temperature for 2 h to remove the physisorbed NH_3. TPD of NH_3 was carried out with a temperature ramp of 10 °C min^{-1}, and the desorption of ammonia was monitored using a thermal conductivity detector (TCD) of a gas chromatograph.

2.4 Catalyst evaluation

Glycerol steam reforming reactions were carried out using a fixed-bed, tubular downflow quartz reactor 18 mm in diameter with a thermocouple 2 mm in width. The reactor was provided with a pre-heater, a syringe pump, a cold condenser and gas flow meter. The catalyst (2 g) was loaded in the middle of the reactor. The reactor was placed in a tubular furnace with an inner diameter of 25 mm. The feed mixture (1 : 3 to 1 : 9 mole ratio of glycerol to water) was fed into the vaporizer using a syringe (B. Braun) pump. The feed entering the pre-heater was maintained at 500 °C before reaching the catalyst bed. A Nippon (NC-2538) temperature controller was used for maintaining the temperature of the pre-heating zone and catalyst bed of the reactor. The conversion of glycerol was calculated from the volume of the condensate. The total gas is measured to understand the glycerol to gaseous product, and the main products H_2, CO_2, CO and CH_4 are analysed by gas chromatography (Shimadzu GC-2014) using a thermal conductivity detector (TCD), Carboxen 1000 column and helium as a carrier gas. The other gas products observed in trace quantities are C_2 products. Liquid products like acetaldehyde, acetone, methanol, and acroline were analysed by GC-MS. Carbon deposition is obtained by weighing the catalysts at the end of the reaction and comparing with carbon from the CHNS analysis.

Glycerol conversion and gas composition are calculated as per the following equations:

$$X_{gly}(\%) = \frac{\text{Gly in} - \text{Gly out}}{\text{Gly in}} \times 100 \quad (2)$$

$$X_{gas}(\%) = \frac{X_{gas}(\mu l)}{\text{Total gas}(\mu l)} \times 100 \quad (3)$$

where X_{gly} (%) = glycerol conversion.

X_{gas} (%) = gas (%), where X is H_2, CO_2, CO and CH_4.

In all the glycerol steam reforming reactions, 6 ml of feed was used. Prior to the reaction, catalysts were reduced using 10% H_2/N_2 at 550 °C/5 h. The evaluation studies were carried out for 25 h time on stream-varying parameters.

3 Results and discussion

3.1 Catalyst characterization

3.1.1 XRD

Fresh catalysts. X-ray diffraction patterns of the catalysts with different loadings of Ni on γ-Al_2O_3 calcined at 500 °C are shown in Fig. 1A. The characteristic peaks of NiO are seen at 2θ of 37.32°, 43.36°, 62.99°, 75.56° and 79.56°, corresponding to (111), (200), (220), (311), and (222) planes of NiO (JCPDS # 75-0197).[33] XRD patterns clearly explain that with an increase in Ni loading on γ-Al_2O_3, the NiO crystallite size increases and calculated from the X-ray line broadening of NiO peak (2θ = 43.36°) using the Scherrer equation and values are shown in Table 1. The NiO particle size varied from 8.5 nm (10NA) to 13.1

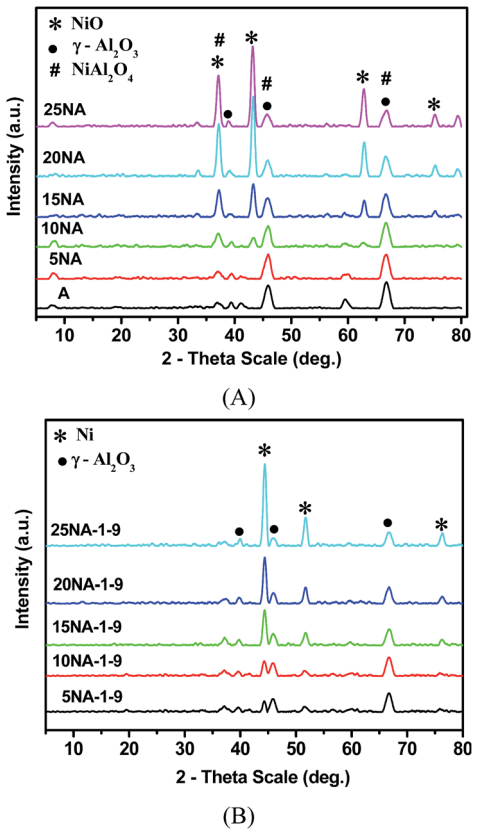

Fig. 1 XRD of Ni/γ-Al_2O_3 (A) calcined catalysts and (B) used catalysts at 650 °C, GWMRs = 1 : 9.

nm (25NA). On the other hand, the diffraction peaks at $2\theta = 39.2°$, 46.2° and 66.9° confirm presence of γ-Al_2O_3. The characteristic peaks of $NiAl_2O_4$ spinel ($2\theta° = 37.32°$, 46.2°, and 66.9°) are very close to that of NiO and γ-Al_2O_3 and cannot be distinguished.

Used catalysts. Diffraction patterns of different Ni-loaded γ-Al_2O_3 catalysts studied for 25 h time on stream at a reaction temperature of 650 °C, and GWMRs (1 : 9) are presented in Fig. 1B. The XRD of all five catalysts show peaks at 44.38°, 51.72°, and 76.2°, and these reflections are assigned to metallic Ni crystallites. Characteristic peaks of γ-Al_2O_3 ($2\theta = 39.2°$, 46.2°, and 66.9°) are also detected in all of the catalysts. The XRD patterns of the 15NA (15 wt% Ni/γ-Al_2O_3) catalyst evaluated in glycerol reforming at different temperatures are presented in Fig. 2A. The characteristic peaks seen at 44.38°, 51.72°, and 76.2° assigned to metallic Ni crystallites are increasing with temperature and the crystallite size is calculated from X-ray line broadening of the Ni peak ($2\theta = 44.38°$), and the values are shown in Table 2.[31,33] The 15NA catalyst is further studied using different GWMRs at 650 °C for 25 h and the diffraction patterns are shown in Fig. 2B. With an increase in steam ratio, a nominal increase in Ni crystalline size is seen. These studies show that the effect of temperature on Ni sintering is more pronounced compared to steam. The reducible NiO phase is observed as the metallic Ni peak in the XRD of all used catalysts. No carbon peak is observed in the XRD of all used catalysts as the carbon deposition is below the XRD detection range. Note that the carbon deposition is detected by CHNS and Raman.

3.1.2 EDAX. The EDAX analysis of fresh samples was carried out to determine nickel content on γ-Al_2O_3, and the data is shown in Table 1. The composition of the Ni loaded on γ-Al_2O_3 catalysts evaluated in glycerol reforming is shown in Table 2. EDAX analysis of Ni-loaded γ-Al_2O_3 used catalysts shows low Ni content compared to calcined catalysts due to carbon deposition. The carbon deposition decreased up to 15NA catalyst, and at higher loadings (20NA and 25NA), carbon deposition increased. When 15NA is studied under different GWMR ratios, the Ni% decreased with decreasing steam. The carbon deposition is also seen as increasing with decreasing steam. The observed decrease in Ni content is due to an increase in the carbon on surface layers, which may change the ratios.

3.1.3 BET surface area. The surface area obtained of γ-Al_2O_3 and both fresh and used Ni/γ-Al_2O_3 catalysts are shown in Table 1 and 2. The surface area of γ-Al_2O_3 is around 192 $m^2\ g^{-1}$, which decreased with an increase in Ni loading.[34] The surface area of the used catalysts also decreased, which may be due to some factors like reaction temperature and carbon deposition. The alumina structure undergoing transition at higher temperatures may reduce the surface area. However, in the interacted aluminas, transitions are slow, and the corresponding textural changes are not observed in XRD. The coke deposited on the surface of the catalyst may block the pores and result in decreased surface areas.[31,35]

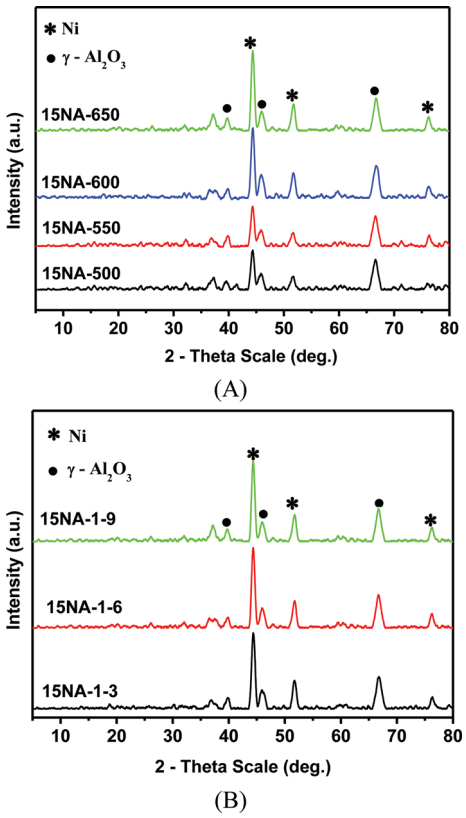

Fig. 2 XRD of 15NA catalyst used (A) at different temperatures (°C) at 1 : 9 GWMRs, and (B) different GWMRs at 650 °C.

3.1.4 CHNS analysis. CHNS analysis was carried out to determine the amount of carbon deposition studied under different reaction conditions, and the data is shown in Table 2. Carbon deposition is more at lower loadings of Ni (5NA and 10NA) due to acid sites available on the γ-Al_2O_3 surface

Table 1 Physical characteristics of Ni/γ-Al_2O_3-calcined catalysts

Catalysts	NiO crystallite size (nm) from XRD	Ni (wt%) by EDAX	BET surface area ($m^2\ g^{-1}$)	H_2 consumption (mmol g_{cat}^{-1})/Ni reducibility[a] (%)	Acidity[b] (μmol g_{cat}^{-1})
A	—	—	192	—	—
5NA	—	4.9	185	0.55/65	300
10NA	8.5	10.2	179	1.14/67	—
15NA	10.1	16.3	175	1.73/68	160
20NA	12.3	21.1	170	2.41/71	—
25NA	13.1	24.2	162	2.98/70	85

[a] H_2 consumption/Ni reducibility (%) from TPR analysis. [b] Acidity from NH_3-TPD analysis.

Table 2 Physical characteristics of Ni/γ-Al_2O_3-used catalysts

Catalysts	Ni crystallite size (nm) from XRD	Elemental composition from EDAX		Carbon (%) from CHNS analysis[a]	BET surface area[b] (m^2 g^{-1})
		Ni%	C%		
5NA-1-9	9.5	3.9	2.5	4.2	165
10NA-1-9	9.8	8.4	2.0	3.8	150
15NA-1-9	10.6	14.1	1.5	3.1	150
20NA-1-9	13.1	18.6	2.5	4.8	140
25NA-1-9	14.9	21.5	3.5	5.9	125
15NA-1-6	10.4	12.3	3.0	7.6	135
15NA-1-3	10.1	11.2	3.8	9.7	120
15NA-600	10.5	13.8	1.6	3.2	—
15NA-550	10.3	13.4	1.8	3.4	—
15NA-500	10.1	13.0	2.0	3.7	—

[a] Standard deviation of carbon = ±0.1%. [b] Standard deviation of BET surface area = ±5.

(Table 1). With increasing Ni content, the acid sites decreased, and less coking is observed on 15NA. However, with the further increase in nickel, coking rate increased. Of all the catalysts studied, the carbon deposition observed is low on the 15NA catalyst, which was studied further at different temperatures, and GWMRs showed more carbon deposition at low temperature and low steam.[36] The reasons are discussed in catalyst evaluation section.

3.1.5 TPR. TPR analyses were performed to investigate the reducibility of Ni^{2+} species present in the calcined catalysts, and the results are shown in Fig. 3 and Table 1. TPR profiles of different Ni-loaded γ-Al_2O_3 catalysts show two distinct reduction processes. A less intense peak is seen between 300 and 350 °C is due to the reduction of Ni^{2+} species that are in weak interaction with the support. A broad high temperature peak in the region of 450–800 °C with T_{max} of reduction around 650 °C that may be seen due to strong interaction Ni^{2+} with γ-Al_2O_3 support.[37,38] At higher Ni loadings (20NA and 25NA), a broad signal is shifted to a lower temperature (550 °C), indicating the presence of Ni^{2+} species with decreased strength of interaction. This indicates that at higher Ni loadings, the support is with heterogeneous distribution of the Ni^{2+} species. The reduction peak appearing at higher temperatures may be attributed to the reduction of Ni^{2+} ions from non-stoichiometric nickel-aluminate species.[16,38]

3.1.6 NH_3-TPD. The ammonia adsorption–desorption technique usually enables one to determine the strength of acid sites present on the surface of catalyst. The TPD of NH_3 profiles of typical Ni/γ-Al_2O_3 catalysts (5NA, 15NA and 25NA) are shown in Fig. 4. Total acidity (300–700 °C) on these decreased with an increase in Ni loading (Table 1).[20]

3.1.7 TEM. The morphology of deposited carbon is studied by TEM and photographs of representative samples are shown in Fig. 5. On the 15NA-1-9 sample (Fig. 5a and b) Ni metal particles are observed as dark spots on the surface of γ-Al_2O_3 support. At higher Ni loadings, *i.e.* on 20NA-1-9 and 25NA-1-9, TEM images show formation of more carbon filaments with dispersed nickel particles (Fig. 5c and d). The glycerol steam reforming reaction over Ni/γ-Al_2O_3 catalyst leads to the formation of graphitic flake-like carbon (filamentous carbon or carbon nanotubes) and amorphous carbon, and the results obtained are in confirmation with the reported literature.[39–41]

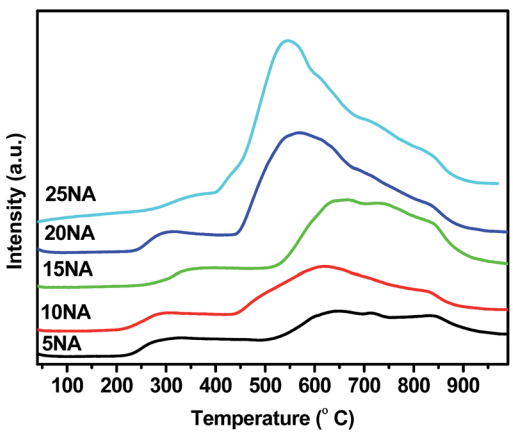

Fig. 3 TPR analysis of Ni-loaded γ-Al_2O_3 catalysts.

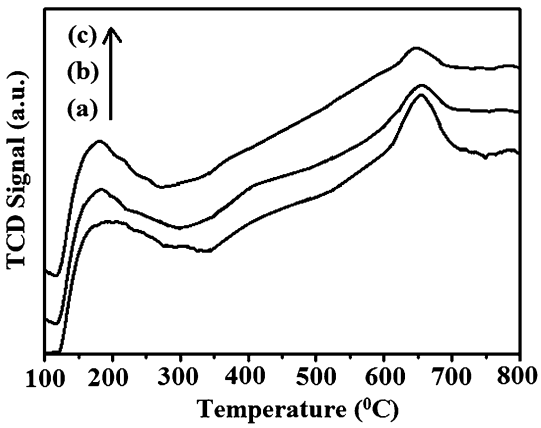

Fig. 4 NH_3-TPD analysis of Ni/γ-Al_2O_3 catalysts: (a) 5NA, (b) 15NA and (c) 25NA.

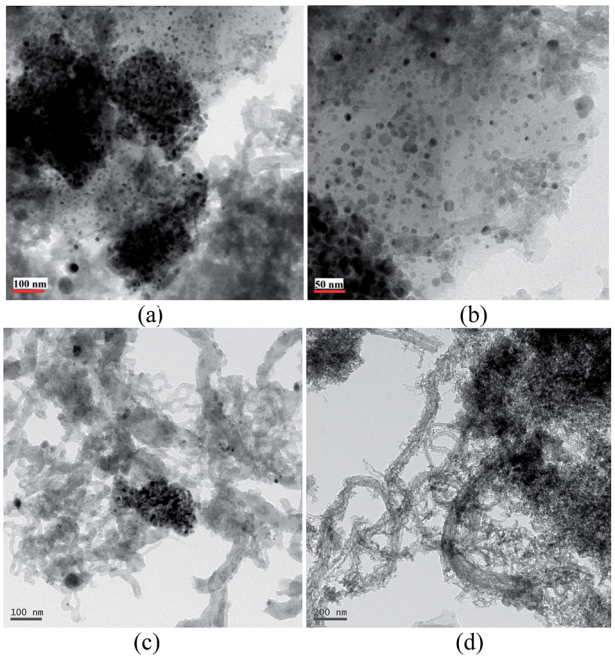

Fig. 5 TEM images of (a) used Ni/γ-Al_2O_3 catalysts and (b) 15NA-1-9, (c) 20NA-1-9, and (d) 25NA-1-9.

3.1.8 Raman spectra. Raman spectroscopy is used to characterize post-reaction catalysts because it is a powerful technique for characterizing the structure of carbonaceous materials. On all catalysts, Raman spectra revealed two broad bands around 1335 cm^{-1} (D band) and 1591 cm^{-1} (G band) (Fig. 6). The former is ascribed to the disordered carbon (amorphous) and the latter is attributed to in-plane carbon–carbon stretching vibrations (E_{2g}) of the graphitic carbon.[39,40,42–43] In all cases, the D band is more intense than the G band, indicating a predominance of disordered carbon. The degree of graphitic carbon deposits can be estimated by the ratio of the area of the D band to that of the G band (I_D/I_G). Note that a higher degree of graphitization produces a lower I_D/I_G ratio. The results indicated that on 15NA disordered carbon and graphitic carbon are minimum as shown in Fig. 6a. The 15NA catalysts are further studied at different GWMRs, and the used catalysts are subjected to Raman spectra as (Fig. 6b). These spectra clearly explain that by decreasing steam, the formation of both types of carbon is seen increasing.[4]

3.2 Catalyst evaluation

3.2.1 Effect of Ni loading on γ-Al_2O_3. Glycerol steam reforming reaction on Ni/γ-Al_2O_3 catalysts is studied at 1 : 9 GWMRs and 650 °C, and the results are shown in Fig. 7. The glycerol conversion and H_2 production rates on 5NA and 10NA catalysts decrease with time on stream.[44] On 15NA catalyst, steady glycerol conversion activity is observed for 25 h. Note that 100% glycerol conversion and 67.5% of H_2 in the gas stream with minimum coking are achieved on this catalyst. At higher Ni loadings (20NA and 25NA) also steady conversion is observed for 15 h, after which the conversion, as well as the H_2 production rate, are showing decreased tendency. On 5NA and 10NA catalysts, activity decreased with time on stream that may be seen as due to the acid sites of alumina available on these catalysts forming coke with time and deactivating the catalyst.[20,25] At a given metal loading, the number of active sites in a catalyst is a function of the metal dispersion. The surface saturation of Ni over γ-Al_2O_3 may be seen around 15% of Ni. The

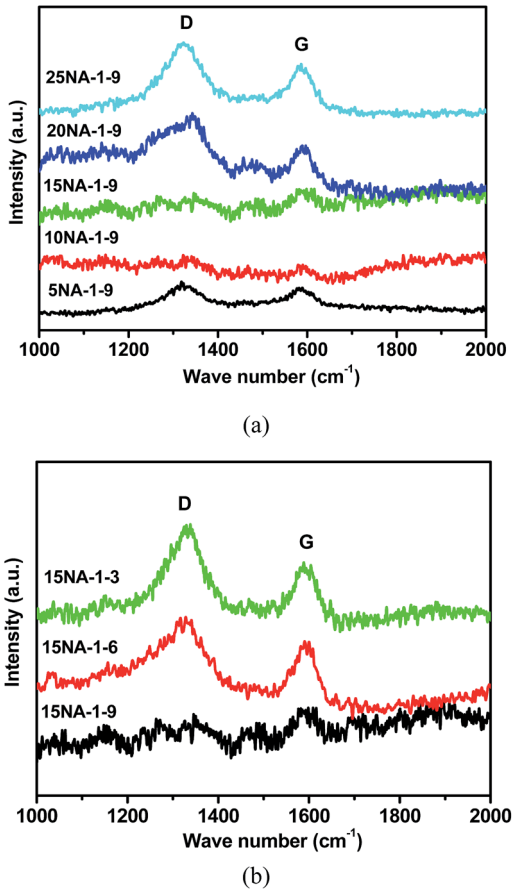

Fig. 6 Raman spectra of used Ni/γ-Al_2O_3 catalysts: (a) different Ni loading at 1 : 9 GWMRs and 650 °C; (b) 15NA catalyst at different GWMRs and 650 °C.

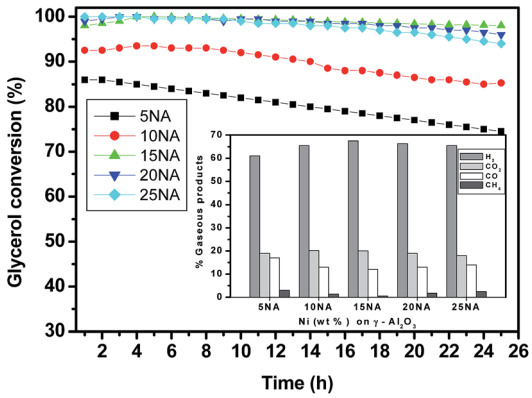

Fig. 7 Effect of Ni (wt%) on γ-Al_2O_3 catalysts in glycerol reforming at 1 : 9 GWMRs and 650 °C. Inset: product gas distribution.

Ni particle formed at this coverage appears to be more suitable for stable activity in glycerol reforming. Above 15% Ni loading, although there is no much difference observed in the particle size of Ni, the TPR clearly shows that the Ni particle formed at higher loading (20NA and 25NA) is reduced relatively at low temperature compared to 15NA. This shows that on 15NA Ni particle is obtained by reducing the interacted Ni (Ni–O–Al). Above this loading, the possibility of formation of free NiO is seen, which may accelerate the Ni particle size affecting the stable activity.[45] Thus, in 15NA, the catalyst is further studied.

3.2.2 Effect of temperature. Glycerol conversion and product gas distribution on 15NA are shown as a function of temperature in Fig. 8. The results show that at 500–600 °C, activity is observed decreasing slightly with time. Below 600 °C due to dehydrogenation and dehydration, the formation byproduct is observed and the side reactions of these byproducts may deposit carbon with time. This is possibly minimised at higher temperatures due to the complete decomposition of glycerol to CO and H_2. Fig. 8 (inset) clearly explains the product gas distributions on 15NA as a function of temperature at 1 : 9 GWMRs. With an increase in temperature from 500 to 650 °C, the glycerol conversion and hydrogen percentages are increased due to the endothermic nature of glycerol steam reforming.[19,44] With an increase in temperature, CH_4 is decreased and CO is increased due to methane steam reforming is favoured at high temperatures.[25] Fig. 9 clearly explains the glycerol conversion and gas product distribution with time on stream on the 15NA catalyst. No change in glycerol conversion is observed for 25 h. However, the decrease in H_2 production, for example 1–2%, a decrease in CO_2 up to 3% and increases in CO up to 6% are observed. The aforementioned results explain that water gas shift reaction decreased with time and building CO concentrations. This may be seen as the loss of active sites due to coking with time.[25,40,46]

3.2.3 Effect of GWMRs. Analysing the effect of the reaction temperature on the catalytic performance of 15NA, a temperature of 650 °C was chosen to study the effect of GWMRs. Moreover, steam reforming is an energy-intensive process, and GWMRs optimization is necessary to minimize the process cost. Thus, glycerol content in the feed was changed, and the results are depicted in Fig. 10. As the GWMRs increased (steam decreased), the glycerol conversion decreased with time due to carbon deposition. The gaseous product distribution also changes, wherein the products H_2 and CO_2 are decreased, and CO and CH_4 are increased due to the absence of a water–gas shift reaction and methane steam reforming.[25,33,44]

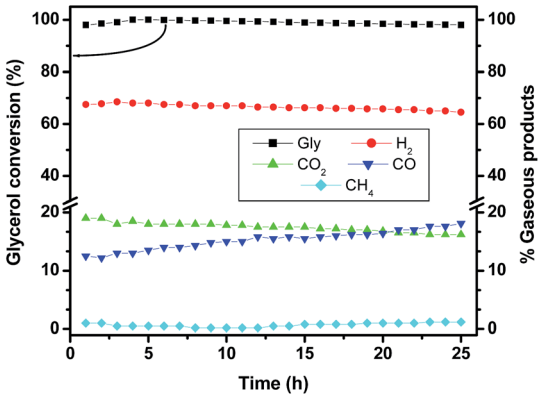

Fig. 9 Time on steam activity on the 15NA catalyst in glycerol steam reforming at 1 : 9 GWMRs and 650 °C.

3.2.4 Coke formation. Coke formation during steam reforming causes rapid deactivation of catalysts and thereby results in low durability. Therefore, it is interesting to determine the reaction conditions to minimize coke formation for the design of efficient carbon resistant catalysts. Fig. 11 represents the carbon formation as a function of Ni loading and GWMRs in glycerol steam reforming.

The carbon deposition is calculated with the following formula:

$$C_{deposition}\ (\text{mg g}^{-1}\ \text{cat. h}^{-1}) = (M_T - M_{cat})/(M_{cat} \times T),$$

where M_T is the total mass of the catalyst and carbon produced after 25 h of reaction, M_{cat} is the mass of the catalyst before reaction, and T is total reaction time (25 h). With an increase of Ni on γ-Al_2O_3, the carbon formation decreases (1.9 to 1.3 mg carbon per g cat. per h); up to 15% Ni and beyond, carbon formation increased to 3.3 mg carbon per g cat. per h. 5NA and

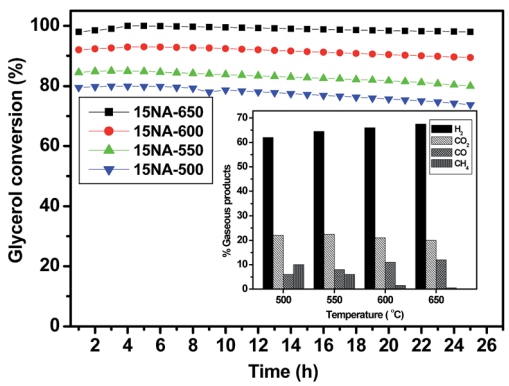

Fig. 8 Effect of temperature on 15NA in glycerol steam reforming; GWMRs = 1 : 9, inset: product gas distribution.

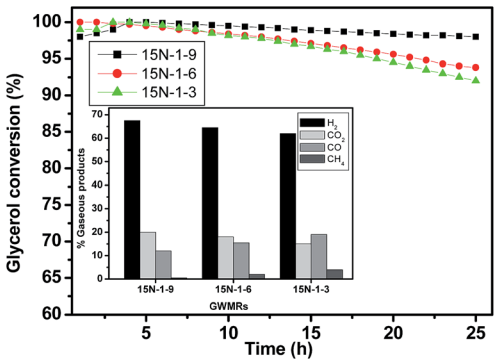

Fig. 10 Effect of GWMRs on the 15NA catalyst in glycerol steam reforming at 650 °C; inset is gaseous product distribution.

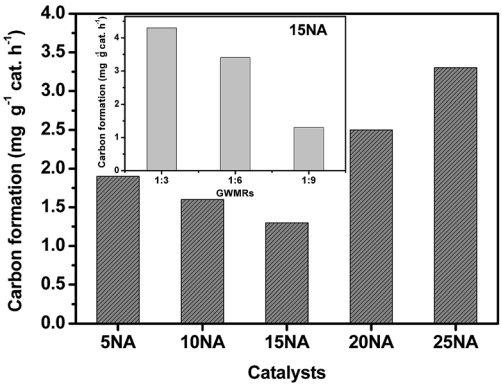

Fig. 11 Effect of Ni loading on γ-Al_2O_3 on the comparison of carbon formation at 650 °C and GWMRs = 1 : 9; inset is carbon formation in different GWMRs on the 15NA catalyst at 650 °C.

10NA show more carbon, indicating the availability of acid sites on alumina supports responsible for coking. Coking is less on 15NA, indicating that the Ni crystallite formed at this concentration is more suitable for reforming (optimum dispersion). Above this loading, on 20NA and 25NA, coking increased due to an increase in the Ni crystallite size. The 15NA catalyst further studied at different GWMRs (Fig. 11 inset) is evaluated for carbon deposition. The carbon formation increased with decreasing steam (1.3–4.3 mg carbon per g cat. per h).

4 Conclusions

Ni/γ-Al_2O_3 catalysts prepared by the impregnation method were evaluated for H_2 production in glycerol steam reforming. The 15 wt% Ni/γ-Al_2O_3 catalyst produced maximum H_2 production and minimum coking with 100% glycerol conversion at 650 °C and 1 : 9 GWMRs. XRD and TPR results are indicating that Ni^{2+} is strongly interacted with γ-Al_2O_3 at low loadings. With increasing Ni loading, the Ni crystallite size increased, and interaction with the support decreased. TPD of NH_3 shows that total acidity of γ-Al_2O_3 support decreased with Ni loading. Raman studies of used catalysts also indicate that surface acidity at lower loadings and Ni crystallite sizes at higher loadings are responsible for coking. The evaluation and characterization of the Ni/γ-Al_2O_3 catalysts clearly establish that Ni^{2+} in strong interaction with γ-Al_2O_3 support resulted in well-dispersed Ni-active sites that are responsible for stable and sustainable activity with minimum coking.

Acknowledgements

Gullapelli Sadanandam thanks CSIR, New Delhi, for an SRF grant, and the authors thank MNRE, New Delhi, for funding the project.

Notes and references

1 C. H. Zhou, J. N. Beltramini, Y. X. Fan and G. Q. Lu, *Chem. Soc. Rev.*, 2008, **37**, 527–549.
2 J. N. Chheda, G. W. Huber and J. A. Dumesic, *Angew. Chem., Int. Ed.*, 2007, **46**, 7164–7183.
3 G. D. Wen, Y. P. Xu, H. J. Ma, Z. S. Xu and Z. J. Tian, *Int. J. Hydrogen Energy*, 2008, **33**, 6657–6666.
4 C. Wu, Z. Wang, P. T. Williams and J. Huang, *Sci. Rep.*, 2013, **3**, 2742, DOI: 10.1038/srep02742.
5 G. Sadanandam, K. Lalitha, V. Durga Kumari, M. V. Shankar and M. Subhramanyam, *Int. J. Hydrogen Energy*, 2013, **38**, 9655–9664.
6 I. Fechete, Y. Wang and J. C. Vedrine, *Catal. Today*, 2012, **189**, 2–27.
7 H. Ziaei-azad, C. X. Yin, J. Shen, Y. Hu and D. Karpuzov, *J. Catal.*, 2013, **300**, 113–124.
8 R. R. Davda, J. W. Shabaker, G. W. Huber, R. D. Cortright and J. A. Dumesic, *Appl. Catal., B*, 2005, **56**, 171–186.
9 P. D. Vaidya and A. E. Rodrigues, *Chem. Eng. Technol.*, 2009, **32**, 1463–1469.
10 Z. Wei, J. Sun, Y. Li, A. K. Datye and Y. Wang, *Chem. Soc. Rev.*, 2012, **41**, 7994–8008.
11 L. P. R. Profeti, E. A. Ticianelli and E. M. Assaf, *Int. J. Hydrogen Energy*, 2009, **34**, 5049–5060.
12 N. J. Luo, J. A. Wang, T. C. Xiao, F. H. Cao and D. Y. Fang, *Catal. Today*, 2011, **166**, 123–128.
13 F. Pompeo, G. Santori and N. Nichio, *Int. J. Hydrogen Energy*, 2010, **35**, 8912–8920.
14 T. Hirai, N. Ikenaga, T. Miyake and T. Suzuki, *Energy Fuels*, 2005, **19**, 1761–1762.
15 G. W. Huber, J. W. Shabaker and J. A. Dumesic, *Science*, 2003, **300**, 2075–2077.
16 A. Iriondo, V. L. Barrio, J. F. Cambra, P. L. Arias, M. B. Guemez and M. C. Sanchez-Sanchez, *Int. J. Hydrogen Energy*, 2010, **35**, 11622–11633.
17 A. M. D. Douette, S. Q. Turn, W. Wang and V. I. Keffer, *Energy Fuels*, 2007, **21**, 3499–3504.
18 A. Iriondo, V. L. Barrio, J. F. Cambra, P. L. Arias, M. B. Guemez, R. M. Navarro, M. C. Sanchez-Sanchez and J. L. G. Fierro, *Top. Catal.*, 2008, **49**, 46–58.
19 S. Adhikari, S. Fernando and A. Haryanto, *Catal. Today*, 2007, **129**, 355–364.
20 S. Li, C. Zhang, P. Zhang, G. Wu, X. Ma and J. Gong, *Phys. Chem. Chem. Phys.*, 2012, **14**, 4066–4069.
21 J. G. Seo, M. H. Youn, S. Park, J. S. Chung and I. K. Song, *Int. J. Hydrogen Energy*, 2009, **34**, 3755–3763.
22 V. Chiodo, S. Freni, A. Galvagno, N. Mondello and F. Frusteri, *Appl. Catal., A*, 2010, **381**, 1–7.
23 I. N. Buffoni, F. Pompeo, G. F. Santori and N. N. Nichio, *Catal. Commun.*, 2009, **10**, 1656–1660.
24 R. L. Manfro, N. F. P. Ribeiro and M. M. V. M. Souza, *Catal. Sustainable Energy Prod.*, 2012, 60–70, DOI: 10.2478/cse-2013-0001.
25 G. Wu, C. Zhang, S. Li, Z. Han, T. Wang, X. Ma and J. Gong, *ACS Sustainable Chem. Eng.*, 2013, **1**, 1052–1062.
26 X. Wang, S. Li, H. Wang, B. Lu and X. Ma, *Energy Fuels*, 2008, **22**, 4285–4291.
27 N. Luo, X. Zhao, F. Cao, T. Xiao and D. Fang, *Energy Fuels*, 2007, **21**, 3505–3512.

28 M. L. Dieuzeide and N. Amadeo, *Chem. Eng. Technol.*, 2010, **33**, 89–96.
29 S. Adhikari, S. Fernando, S. R. Gwaltney, S. D. Filip To, R. Mark Bricka and P. H. Steele, *Int. J. Hydrogen Energy*, 2007, **32**, 2875–2880.
30 C. C. R. S. Rossi, C. G. Alonso, O. A. C. Antunes, R. Guirardello and L. Cardozo-Filho, *Int. J. Hydrogen Energy*, 2009, **34**, 323–332.
31 G. Sadanandam, N. Sreelatha, M. V. Phanikrishna Sharma, S. Kishta Reddy, B. Srinivas, K. Venkateswarlu, T. Krishnudu, M. Subrahmanyam and V. Durga Kumari, *ISRN Chem. Eng.*, 2012, **2012**, 1–10, DOI: 10.5402/2012/591587.
32 V. Durga Kumari, M. Subrahmanyam, A. Ratnamala, D. Venugopal, B. Srinivas, M. V. Phanikrishna Sharma, S. S. Madhavendra, B. Bikshapathi, K. Venkateswarlu, T. Krishnudu, K. B. S. Prasad and K. V. Raghavan, *Catal. Commun.*, 2002, **3**, 417–424.
33 K. Kamonsuangkasem, S. Therdthianwong and A. Therdthianwong, *Fuel Process. Technol.*, 2013, **106**, 695–703.
34 E. Salehi, F. S. Azad, T. Harding and J. Abedi, *Fuel Process. Technol.*, 2011, **92**, 2203–2210.
35 C. Wang, B. Dou, H. Chen, Y. Song, Y. Xu, X. Du, L. Zhang, T. Luo and C. Tan, *Int. J. Hydrogen Energy*, 2013, **38**, 3562–3571.
36 C. Wang, B. Dou, H. Chen, Y. Song, Y. Xu, X. Du, T. Luo and C. Tan, *Chem. Eng. J.*, 2013, **220**, 133–142.
37 M. L. Dieuzeide, V. Iannibelli, M. Jobbagy and N. Amadeo, *Int. J. Hydrogen Energy*, 2012, **37**, 14926–14930.
38 A. Iriondo, J. F. Cambra, M. B. Guemez, V. L. Barrio, J. Requies, M. C. Sanchez-Sanchez and R. M. Navarro, *Int. J. Hydrogen Energy*, 2012, **37**, 7084–7093.
39 D. Z. Mezalira, L. D. Probst, S. Pronier, Y. Batonneau and C. Batiot-Dupeyrat, *J. Mol. Catal. A: Chem.*, 2011, **340**, 15–23.
40 I. Rossetti, A. Gallo, V. D. Santo, C. L. Bianchi, V. Nichele, M. Signoretto, E. Finocchio, G. Ramis and A. D. Michele, *ChemCatChem*, 2013, **5**, 294–306.
41 S. P. Chai, S. H. S. Zein and A. R. Mohamed, *National Postgraduate Colloquim*, School of Chemical Engineering University of Sains Malaysia, Seri Ampangan, 2004, pp. 60–69.
42 A. E. Galetti, M. F. Gomez, L. A. Arrua and M. C. Abello, *Appl. Catal., A*, 2008, **348**, 94–102.
43 M. E. Doukkali, A. Iriondo, P. L. Arias, J. F. Cambra, I. Gandarias and V. L. Barrio, *Int. J. Hydrogen Energy*, 2012, **37**, 8298–8309.
44 V. Dhanala, S. K. Maity and D. Shee, *RSC Adv.*, 2013, **3**, 24521–24529.
45 S. Narayanan and K. Uma, *J. Chem. Soc., Faraday Trans. 1*, 1985, **81**, 2133–2144.
46 E. A. Sanchez and R. A. Comelli, *Int. J. Hydrogen Energy*, 2012, **37**, 14740–14746.